Bioinformatics, 32(16), 2016, 2490–2498
doi: 10.1093/bioinformatics/btw172
Advance Access Publication Date: 1 April 2016
Original Paper

Bioimage informatics

2dSpAn: semiautomated 2-d segmentation, classification and analysis of hippocampal dendritic spine plasticity

Subhadip Basu[1,*], Dariusz Plewczynski[2], Satadal Saha[3], Matylda Roszkowska[4], Marta Magnowska[4], Ewa Baczynska[4] and Jakub Wlodarczyk[4,*]

[1]Department of Computer Science and Engineering, Jadavpur University, Kolkata 700032, India, [2]Center of New Technologies, University of Warsaw, Warsaw, Poland, [3]Department of Electronics and Communication Engineering, MCKV Institute of Engineering, Howrah 711204, India and [4]Department of Molecular and Cellular Neurobiology, Nencki Institute of Experimental Biology, Polish Academy of Sciences, Warsaw, Poland

*To whom correspondence should be addressed.

Associate Editor: Robert Murphy

Received on October 2, 2015; revised on March 21, 2016; accepted on March 26, 2016

Abstract

Motivation: Accurate and effective dendritic spine segmentation from the dendrites remains as a challenge for current neuroimaging research community. In this article, we present a new method (2dSpAn) for 2-d segmentation, classification and analysis of structural/plastic changes of hippocampal dendritic spines. A user interactive segmentation method with convolution kernels is designed to segment the spines from the dendrites. Formal morphological definitions are presented to describe key attributes related to the shape of segmented spines. Spines are automatically classified into one of four classes: Stubby, Filopodia, Mushroom and Spine-head Protrusions.

Results: The developed method is validated using confocal light microscopy images of dendritic spines from dissociated hippocampal cultures for: (i) quantitative analysis of spine morphological changes, (ii) reproducibility analysis for assessment of user-independence of the developed software and (iii) accuracy analysis with respect to the manually labeled ground truth images, and also with respect to the available state of the art. The developed method is monitored and used to precisely describe the morphology of individual spines in real-time experiments, i.e. consequent images of the same dendritic fragment.

Availability and Implementation: The software and the source code are available at https://sites.google.com/site/2dspan/ under open-source license for non-commercial use.

Contact: subhadip@cse.jdvu.ac.in or j.wlodarczyk@nencki.gov.pl

Supplementary information: Supplementary data are available at *Bioinformatics* online.

1 Introduction

Neuronal cells in different brain regions are covered with dendritic spines (Ramon and Cajal, 1904), which are small membranous protrusions having a length of around few microns. They form the postsynaptic compartment of most excitatory synapses in the central nervous system (Bourne and Harris, 2008). Dendritic spine is usually composed of a spine head and a spine neck that connects the spine head to the dendritic shaft (Gray, 1959). More specifically, a spine head, where the excitatory synapse is located, is separated from the parent dendrite by a thin neck, isolating the spine cytoplasm from the dendrite (Harris, 1994). Spines are likely to play an essential role in neural circuits but their exact function is still a matter of debate (Sala and Segal, 2014; Shepherd, 1996; Yuste, 2011).

Because of their morphology, dendritic spines are assumed to play a role in electrical and biochemical compartmentalization (Bonhoeffer and Yuste, 2002; Lee *et al.*, 2012; Tønnesen *et al.*, 2014; Yuste *et al.*, 2000).

Synaptic plasticity is essential for brain development and higher brain functions (Alvarez and Sabatini, 2007; Holtmaat and Svoboda, 2009). Changes in dendritic spine morphology are believed to associate synaptic plasticity (Holtmaat and Svoboda, 2009; Matsuzaki *et al.*, 2004; Oh *et al.*, 2013; Tønnesen *et al.*, 2014; Yuste and Bonhoeffer, 2001), which seem to be critical for synaptic function (Matsuzaki *et al.*, 2001; Nusser *et al.*, 1998). However, the understanding of the relationship between the changes in dendritic spine structure and synapse functions remains inadequate. The quantitative contribution of spine morphology to biochemical compartmentalization is still unknown, in spite of being a long-standing hypothesis (Chang, 1952; Crick, 1982). Therefore, the important question is, whether or how much the synaptic strength may be adjusted through structural changes in spine necks (or the complete spine) (Araya *et al.*, 2014). Effective solution to this problem is particularly difficult due the complex morphology of the dendritic spines. The problem gets compounded with the limited resolution of optical microscopic images (Papa *et al.*, 1995). In many situations, the spines are difficult to be segmented from the images of dendritic segments having hundreds of these protrusions. Identification of true spine boundaries is difficult and time-consuming (Mishchenko *et al.*, 2010; Mukai *et al.*, 2011; Son *et al.*, 2011). Accurate quantitative analyses of the spines depend on the question, 'how easily and effectively the spines can be segmented from the dendrite?'

Recently, some researchers have tried to address the earlier issue. A Patent Cooperation Treaty (PCT) application (Wong *et al.*, 2006) presents a method for characterizing one or more neurons comprising dendritic spines utilizing a grassfire process. The technique is particularly efficient for detecting separated spine heads. However, no detailed description is provided on how to precisely detect the contours of the spine. The work by Ruszczycki *et al.* (2012a,b) presents a method for segmentation and analysis of every spine separately using a contour tracing algorithm. Two points are marked for each spine, one at the bottom of the neck and the other at the head [the farthest point (FP) on the spine from the neck]. Then a parameterized contour tracing algorithm detects the spine boundary and the morphological attributes. This process requires extensive user-intervention. In images with hundreds of spines, marking two end-points and choosing appropriate segmentation parameters for every spine is a rigorous job. This makes segmentation of dendritic spines both times consuming and error-prone. In one of the recent developments, Heck *et al.* (2015) proposed an advanced 3D approach for segmentation of the spines, however, that kind of approach requires many optimization steps and extensive manual supervision.

Apart from the works mentioned earlier, several neuromorphological tracing tools are also available (Donohue and Ascoli, 2011). Many of these techniques use the commercial reconstruction software *Neurolucida* (Halavi *et al.*, 2012). Existing tracing tools like, *Filament Tracer (http://www.bitplane.com/imaris/filamenttracer), Amira (http://www.fei.com/software/amira-3d-for-life-sciences/), Eutectic NTS (http://neuronland.org/NLMorphologyConverter/MorphologyFormats/Eutectics/Spec.html), 3DMA-Neuron (http://www.ams.sunysb.edu/~lindquis/3dma/3dma_neuron/3dma_neuron.html), NeuronJ (http://www.imagescience.org/meijering/software/neuronj/), NeuronStudio (https://en.wikipedia.org/wiki/NeuronStudio), Neuron_Morpho (http://www.southampton.ac.uk/~dales/morpho/), etc.* require extensive manual annotations and parameter selection for automated/semiautomated reconstructions. For example, *Filament Tracer* (a module of the commercial *Imaris* software) incorporates visualization and editing utilities and performs morphometric calculations by fitting the objects from the finite list of shapes (such as, cone, ball and cylinder). Similarly, *Neuron_Morpho*, an open-source tool for semiautomatic digital tracing of neurons from image stacks, generates outline of the neurite or soma by drawing straight lines across the width of the section. None of these applications provides formal morphological definitions of spines. Some applications like *NeuronJ* are developed as *ImageJ* (Abràmoff *et al.*, 2004) plugins and are slow in analyzing images. These tools are often applicable on specific types of images, like, 8-bit grayscale or indexed color images.

The proposed 2dSpAn method significantly reduces human involvement and allows the operators to quantitatively assess dendritic spine plasticity. Users need to mark a specific dendritic segment, automatically segment the spines using the designed convolution kernels and finally mark the spines of interest to extract relevant features with high accuracy and minimal intervention. Moreover, the proposed 2dSpAn method allows morphological analysis of spines from different type of images including those acquired by super-resolution, confocal and wide field microscopy images.

The overall method is divided in two steps: (i) segmentation of the dendritic spines and (ii) quantitative assessment of spine morphology. In the article, we briefly describe the theory behind the developed segmentation algorithm and highlight the main features of the 2dSpAn interface and software architecture. The performed experimental validation is done with respect to the confocal images of dendritic spines from dissociated hippocampal cultures. Finally, we conclude with a discussion on open-source software development, limitations and future plans.

2 Theory and methods

Present work considers a 2D grayscale image (I) of dendrites with spines as the input to the segmentation method. In I, dendrites with the spines are defined as the object region ($\mathcal{O}$) and the region ($I - \mathcal{O}$) is considered as the background (B). For segmentation of the dendritic spines, a dendritic segment is first identified by marking the two points p, q in $\mathcal{O}$. We then estimate the region of interest (ROI) around p, q as R, such that $R \subseteq I$. We have used adaptive binarization algorithm (Otsu, 1975) in R to segment $\mathcal{O}$ from B (Fig. 1).

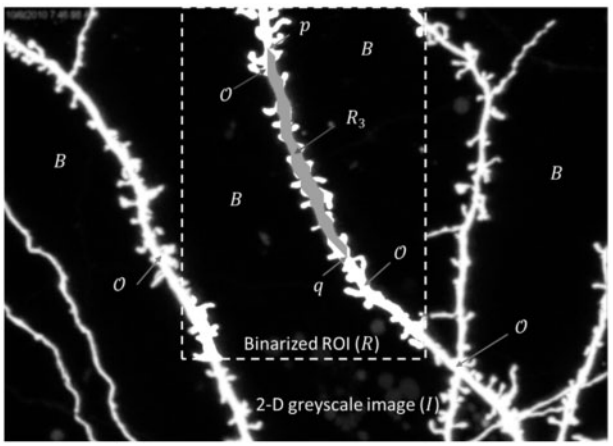

Fig. 1. A grayscale image (I) with dendrites and spines, along with the object region ($\mathcal{O}$) and the background (B). The ROI (R) is identified by manually selecting the points (p, q) in $\mathcal{O}$ and binarized using adaptive thresholding. R_3 is the segmentation result obtained after applying the complementary convolution kernels with $\alpha = 45$

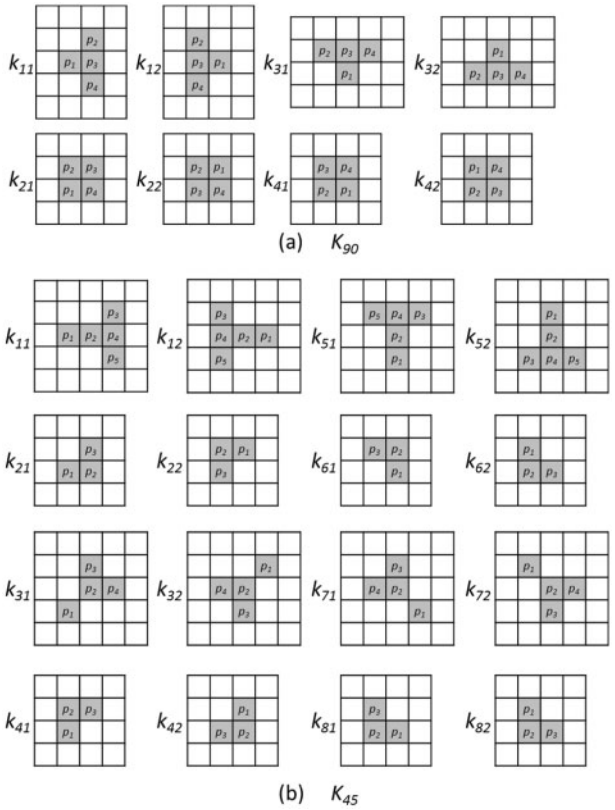

Fig. 2. Convolution kernels (K_α) for (**a**) $\alpha = 90$ and (**b**) $\alpha = 45$

Moreover, previously we have designed a set of convolution kernels (Basu *et al.*, 2007), for segmentation of the dendritic spines in R.

Convolution kernels (K_α) are represented as mutually exclusive set of 3-tuples, such that, $K_\alpha : \{(\alpha, k_{11}, k_{12}),\ (\alpha, k_{21}, k_{22}) \ldots (\alpha, k_{M1}, k_{M2})\}$, where α represents the *angular spread* (in degree) of the kernel and $M = 360/\alpha$. Designed convolution kernels with $\alpha = 90$ and $\alpha = 45$ are shown in Figure 2a and b. During the segmentation process, we first apply the kernel k_{i1} from p until q or a boundary condition is reached. Let the expanded region in this step be $R_1 \subset \mathcal{O}$ [Fig. 3(a–e)]. Then k_{i2} is applied from q until p or a boundary condition is reached. Let the region expanded after applying k_{i2} be $R_2 \subset \mathcal{O}$ (Fig. 3f and g). Then, we estimate, $R_3 = (R_1 \cap R_2)$ as the intersection of the two expanded regions generated by the two kernels, k_{i1} and k_{i2} (Fig. 3h). We then manually select a spine seed s_k as a point inside a potential dendritic spine region, bounded by B and R_3 (Fig. 3h). The bounded region, expanded from s_k using a region growing algorithm (Adams and Bischof, 1994), is marked as segmented spine (S_k) (Fig. 3i). Variation of segmentation results with different choices of α, and varying binarization thresholds are illustrated in Figure 4(a–g). The rationale behind the choice of the segmentation kernels is included in supplementary.

2.1 Quantitative assessment of spine morphology

The morphology of the dendritic spines is complex and difficult to segment and quantify. In most cases, they are described by simple parameters like *length* and *head width* (Ruszczycki *et al.*, 2012a,b). However, high resolution confocal microscopy allows visualization of the complex structures in greater details. In this work, we have attempted to define key morphological attributes from the 2D images of dendritic spines and classify the segmented spines in four categories; (a) Stubby, (b) Mushroom, (c) Filopodia and (d) Spine-head Protrusion (see Fig. 5 for illustration). Specifically, we propose formal definitions of the *base*, *neck* and *head* of the spine, using the standard mathematical notations of digital topology and geometry. First, we identify the base (B_k) of the dendritic spine S_k as the set of points (S_{base}) in R_3 such that S_{base} and S_k are adjacent. Please note that, 8 – *neighbourhood* of a point is used to define the adjacency criterion.

Definition 1: The *central base point* (CBP) is defined as $\text{CBP}_k = \frac{1}{|B_k|}\sum_i p_i$; where, $|B_k|$ is the cardinality of the set of points in B_k, $\text{CBP}_k \in (R_3 \cup S_k)$ and $p_i \in B_k$.

Now, we compute distance transform (DT) (Borgefors, 1986; Saha *et al.*, 2015) in R by considering $S_k$as the object and $(R - S_k)$ as background. Let the DT values (distance of each point from the background) for any point (p) in R be $\Omega(p)$. We use *local scale* of an object pixel as the DT value (depth) at the closest locally deepest pixel. Specifically, a pixel $p \in S_k$ is said to be *locally deepest* if $\forall q \in \mathcal{N}_l(p)$, $\Omega(q) \leq \Omega(p)$, where $\mathcal{N}_l(p)$ is the $(2l+1)^2$ neighborhood of p; here, $l = 2$ is used to avoid noisy local maxima. To find the length of the spine, from the FP to CBP_k in S_k, we compute DT in S_k by considering CBP_k as background and represent it as $\widehat{\Omega}$.

Definition 2: The *central head point* (CHP) is defined as $\text{CHP}_k = \frac{1}{|HP_k|}\sum_i p_i$, where, $\text{HP}_k \subset S_k$ be the set of all locally deepest pixels in S_k, $|HP_k|$ is the cardinality of the set of points in HP_k, $\text{CHP}_k \in S_k$ and $p_i \in \text{HP}_k$.

Definition 3: The *FP*, $p \in S_k$, is defined such that, $\forall q \in S_k$, $\widehat{\Omega}(q) \leq \widehat{\Omega}(p)\}$.

Please note that, CBP, CHP and FP play key roles in estimation of the spine attributes like, *length of the spine*, *neck-length*, *neck-width*, *head-width*, etc. To estimate these features, we further extend the earlier definitions to find the geodesic path from *base to head* (BH_k) of the spine S_k by joining the two central points CBP_k and CHP_k such that $\sum_{p_i \in \text{BH}_k} \Omega(p_i)$ is minimized (Fig. 6a and b). Likewise, we compute the central path from *head to farthest point* (HF_k) of the spine S_k by joining CHP_k and FP_k, such that $\sum_{p_i \in \text{HF}_k} \Omega(p_i)$ is minimized (Fig. 6a and b).

Now, we estimate the neck length of S_k as $\text{NL}_k = \text{BH}_k - \Omega(\text{CHP}_k)$. *Minimum neck-width* (MNW) of S_k is estimated as $\text{MN W}_k = \min_{\forall p_i \in \text{BH}_k}(\Omega(p_i))$. *Average head-width* (AHW) of the spine S_k is estimated as $\text{AHW}_k = \text{avg}_{\forall p_i \in \text{HP}_k}(\Omega(p_i))$ and the *length of the spine* S_k is estimated as, $L_k = |\text{BH}_k| + |\text{HF}_k|$.

Algorithm 1. 2dSpAn spine classification algorithm

Input: S : *set of segmented spines in* R, *such that* $R \subseteq I$
Output: *Classification of each* $S_k \in S$ *as Stubby, Filopodia, Mushroom or Spine – head Protrusion*

for (*each segmented spine* $S_k \in S$) **do**
{*if* $(\text{NL}_k == 0)$ *then*
$S_k = Stubby$
if $\left((\text{NL}_k > 0)\&\&\left(\frac{D_{\max}(\text{HP}_k)}{L_k} > \gamma\right)\right)$*then* $S_k = Filopodia$
if $\left((\text{NL}_k > 0)\&\&(S_k \neq Filopodia)\&\&\left(\frac{\text{BH}_k}{L_k} < \delta\right)\right)$*then*
$S_k = Mushroom$
if $((\text{NL}_k > 0)\&\&(S_k \neq Filopodia)\&\&(S_k \neq Mushroom))$ *then*
$S_k = Spine - head\ Protrusion$
}**end for**

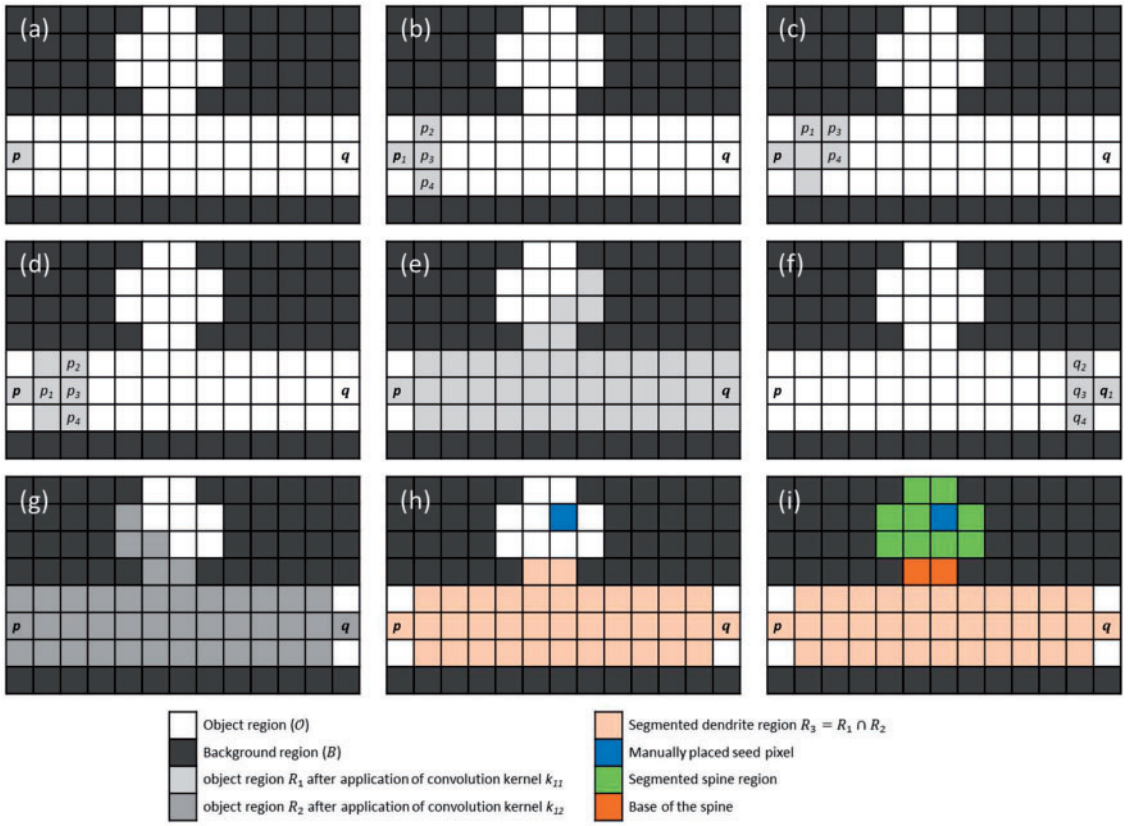

Fig. 3. A step-by-step representation of the segmentation process over a synthetic dataset, by applying the convolution kernel $K_{90} = \{(90, k_{11}, k_{12})\}$; (**a**) the start ($p$) and end ($q$) points are marked on a synthetic dataset, (**b**) the convolution kernel k_{11} is first applied on p, (**c and d**) results of successive application of the convolution kernel k_{11}, on p_2 and p_3, respectively, marked in (b), (**e**) result obtained after iterative application of k_{11} on the image (stop, when q is reached or no further application of the kernel is possible), (**f**) now, the convolution kernel k_{12} is first applied on q, (**g**) result obtained after iterative application of k_{12} on the image, (**h**) the segmented dendrite region (R_3) is estimated by intersection of the regions generated by k_{11} and k_{12}, a manual seed point is then placed inside the potential spine region, (**i**) the spine region is segmented using region growing from the manual seed and the base pixels are identified following the Definition 1

2.2 Classification of the segmented spines

Using the morphological definitions discussed in Subsection 2.1, we classify the spine shapes into one of the four categories: Stubby, Mushroom, Filopodia and Spine-head Protrusion. Formal morphological definitions for these spine categories are not available in the literature and these classifications were largely subjective and decided empirically by the experimental biologists. To address this issue, we have developed a rule-based approach for automatic categorization of the spine shapes into one of the four classes as discussed in Algorithm 1, where, $0 \leq \gamma, \delta \leq 1$ and $D_{\max}(\mathrm{HP}_k)$ is the distance between the two farthest locally deepest points (HP_k) in S_k.

The basic classification logic relies on the accurate estimation of the *neck length* (NL_k) of a spine. If the *neck length* is zero, we classify a spine as Stubby. Otherwise, we check the positions of the locally deepest points (HP_k). In case of a thin, Filopodia, the locally deepest points are usually spread along the length (L_K) of the spine. This is not common in Mushroom or Spine-head Protrusions, where the locally deepest points are usually concentrated around the *spine-head* regions. Therefore, the ratio $D_{\max}(\mathrm{HP}_k)/L_k$ returns higher values in case of a Filopodia. Then, to classify the Mushroom type spines we estimate the *base-to-head* distance (BH_k) of a spine. We have observed that the Mushroom spines have short *base-to-head* distance in comparison to the overall *length of spine* and the ratio BH_k/L_k decisively classifies the Mushroom spines from the Spine-head Protrusions. Spine classification results on different dendritic segments with $\gamma = 0.5$ and $\delta = 0.5$ are shown in Figure 7.

3 Results

The developed 2dSpAn tool is useful in a variety of applications involving large-scale annotation of dendritic spines for quick and accurate assessment of spine plastic changes. There are two specific challenges involved in this process: (i) accurate segmentation of individual spines from the dendritic segment and (ii) quantitative analysis of spine morphology for effective assessment of dendritic spines' structural changes. As discussed before, the objective of this work is to demonstrate the efficacy of the 2dSpAn tool in annotation of dendritic spines and to compare its performance with respect to the available tools. Specifically, we have concentrated on the analysis of spine plasticity using the morphological features presented in the previous section. The confocal light microscopy images of dendritic spines from dissociated hippocampal cultures have been used for: (i) quantitative analysis of spine morphological changes, (ii) reproducibility analysis for assessment of user-independence of the developed software,(iii) accuracy analysis with respect to the ground truth (GT) annotations generated by the experimental biologists and also with respect to the available *state of the art*. In the following subsection, we first describe the image acquisition protocol and the image sets used for the experimental validation. Then, we present the analysis of spine structural changes of the mentioned datasets, mutually blind three-user reproducibility analysis using the developed 2dSpAn software and finally, the error analysis with respect to the GT annotations and also with respect to the work by Ruszczycki *et al.* (2012a,b).

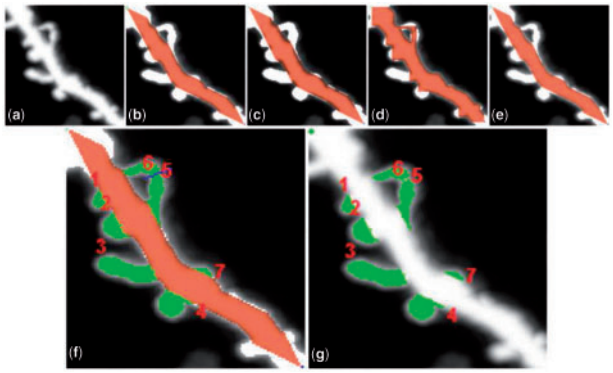

Fig. 4. Variation of segmentation results with different choices of α and binarization thresholds (Th); (**a**) original image segment, (**b**) $\alpha = 45$ with adaptive Th = 128, (**c**) $\alpha = 45$ with Otsu Th = 98, (**d**) $\alpha = 90$ with adaptive Th = 128, (**e**) $\alpha = 45$ with custom Th = 160, (**f**) spines are segmented using the image obtained in (e) by clicking once on each spine (please note that the connected spines #5 and #6 are segmented by a 'Blue' line using the 'Manual Seg' tool), (**g**) final spine segmentation result obtained from (f)

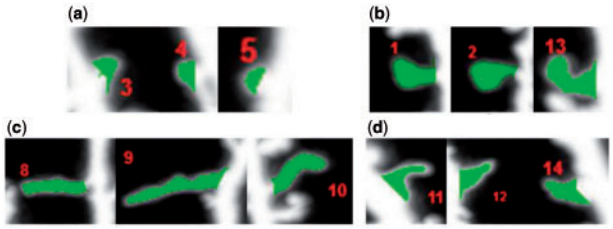

Fig. 5. Different examples of dendritic spine categories; (**a**) Stubby, (**b**) Mushroom, (**c**) Filopodia and (**d**) Spine-head Protrusion (Color version of this figure is available at *Bioinformatics* online.)

3.1 Description of the dataset

3.1.1 Dissociated hippocampal cultures preparation

Dissociated hippocampal cultures from P0 (postnatal Day 0) Wistar rats were prepared as described later. Brains were removed and hippocampi were isolated on ice in dissociation medium DM; 81.8 mM Na_2SO_4, 30 mM K_2SO_4, 5.8 mM $MgCl_2$, 0.25 mM $CaCl_2$, 1 mM HEPES pH 7.4, 20 mM glucose; 1 mM kynureic acid; 0.001% Phenol Red. Next, hippocampi were incubated twice for 15 min at 37°C with 100 units of papain (Worthington, NY) in DM, then rinsed three times in DM and subsequently three times in plating medium [MEM, 10% fetal bovine serum and 1% penicilin-streptomycin]. Hippocampi were triturated in plating medium, then centrifuged for 10 min at room temperature, at 208.5 *g*. The resulting cell pellet was suspended in plating medium, cells were counted and plated at density 120 000 cells per 18-mm-diameter coverslip (Assistent, Germany) coated with 1 mg/ml poly-L-lysine (Sigma) and 2.5 μg/ml laminin (Roche). At 3 h after plating medium was exchanged for maintenance medium (Neurobasal-A without Phenol Red, 2% B-27 supplement, 1% penicillin-streptomycin, 0.5 mM glutamine, 12.5 μM glutamate, 25 μM β-mercaptoethanol) and cells were kept at 37°CC, under a humidified 5% CO_2 atmosphere.

3.1.2 Live cell imaging and chemical long-term potentiation (cLTP) stimulation

Cultured hippocampal neurons were transfected at 14 days in vitro (DIV) with Syn-GFP plasmid to visualize neuronal morphology. Live cell imaging was performed on 20–22 DIV. Prior the imaging, the cells were placed in an acquisition chamber with controlled temperature (37°C) and stable CO_2 (5%) concentration. Dendritic segments decorated with dendritic spines were imaged at the Time 0, before stimulation, and then was induced by bath application of a mixture of 50 μM forskolin, 50 μM picrotoxin and 0.1 μM rolipram (each dissolved in DMSO) in maintenance media. Dendritic segments were imaged at 10 min after cLTP induction. Images were acquired using the Carl Zeiss LSM780 confocal microscope with a C-Apochromat 40×/1.2 NA water immersion objective using 488 nm wavelength argon laser at 3% transmission at 70 nm/pixel resolution. A series of z-stacks were acquired at 0.4 μm step.

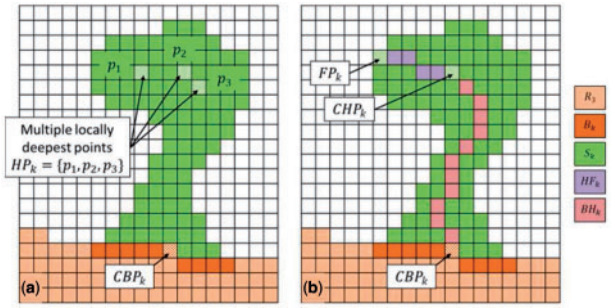

Fig. 6. Key structural points in a spine; (**a**) Multiple locally deepest points are identified as $HP_k = \{p_1, p_2, p_3\}$, such that $D_{max}(HP_k)$is the distance between the two farthest locally deepest points (p_1, p_3) and the CHP is identified as the center of $\{p_1, p_2, p_3\}$, (**b**) the key morphological points, CBP_k, CHP_k and FP_k, and the two geodesic paths BH_k and HF_k between these points in a spine S_k are shown

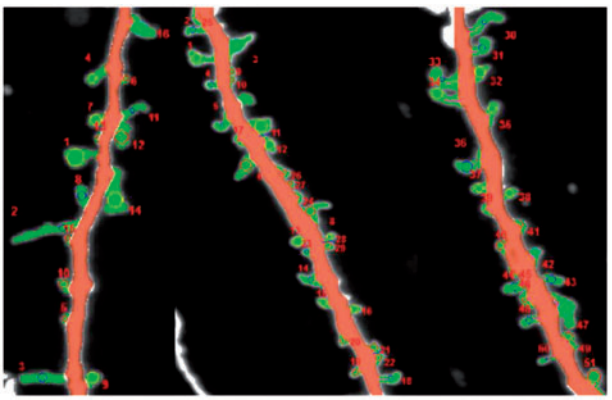

Fig. 7. Spine classification results on three dendritic segments. The circle represents the AHW of the spine $S_k$at the central head-point. The red, yellow, blue and cyan colors of the circle represent the four spine classes, Stubby, Mushroom, Filopodia and Spine-head Protrusion, respectively

3.1.3 Dataset preparation and nomenclature

Nine different neurons from rat dissociated hippocampal cultures were imaged using a confocal light microscope, before and after cLTP. All the images were captured twice, one at baseline (before cLTP stimulation) and the other after 10 min from cLTP induction. During image preprocessing, we took maximum intensity projection (MIP) of the confocal z-stack and perform Gaussian de-noising on the 2D MIP image. The preprocessed MIP images at Time 0 is labeled as T0 and the images captured after 10 min are labeled as T10. In this experiment, total 459 dendritic spines are manually segmented and annotated by experimental biologists in both T0 and T10 images using an open-source image analysis software, Fiji (Schindelin *et al.*, 2012).

3.2 Analysis of spine plasticity

For detailed quantitative analysis of the dendritic spines, first we have analyzed the 2dSpAn classification results of 459 segmented spines obtained from nine sets of T0 and T10 images. Initially in T0, ~31% were classified as Stubby (S), ~32% as Filopodia (F), ~27% as Mushroom (M) and the rest 10% as Spine-head Protrusions (P). After imaging of the same spines 10 min after cLTP (in T10), we got ~35% Stubby spines, ~33% Filopodia, ~23% Mushroom and ~9% Spine-head Protrusion spines. More than half of the spines (~54%) remain in the same state 10 min after cLTP induction. The transition patterns of spines are illustrated in Figure 8a. The transition patterns among three types of spine categories, Stubby, Mushroom and Filopodia (by combining Spine-head Protrusions with Filopodia) are shown in Figure 8b.

To further investigate the relative changes in various morphological attributes of the segmented spines, two important features, *area* and *length* are considered from the overall experiment (Supplementary Fig. S1). Please note that, the method allowed to record noticeable changes in *area* and *length* of dendritic spines, the two most important attributes for spine plasticity, during cLTP induction. In the previous section, we have morphologically defined the *neck-length* attribute, and used this feature to classify the Stubby spines (when *neck-length* is zero). In T0, the initial population of some Stubby spines remains in the same state, whereas some get transformed to Filopodia or Mushroom. On the other hand, some Filopodia spines in T0 became Mushroom in T10. All these activities are reflected in the changes of *length* and *neck-length* attributes (Supplementary Fig. S2). Likewise, the variations in average *neck-width* along the neck region of the segmented spines are also observed during the experiment. Stubby spines are excluded in this analysis since they do not have any neck region. *Head-width* estimates are important for all spine categories. The changes in *neck width* and *head-width* for all Mushroom spines at T10 are included in Supplementary Figure S3.

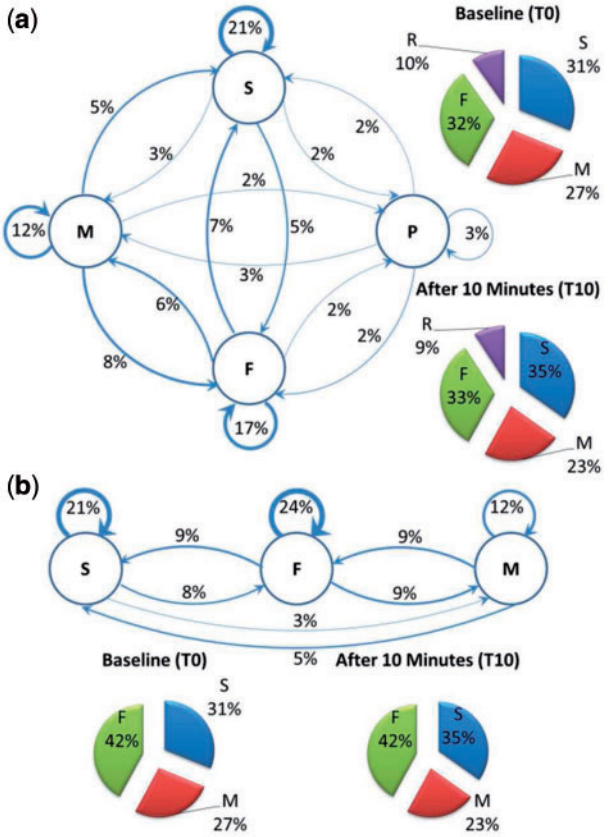

Fig. 8. Analysis of spine plasticity using automatic spine classification results, where S, F, M and P represent spine categories: Stubby, Filopodia, Mushroom and Spine-head Protrusions, respectively. The numbers and the edge thickness represent relative transition (in % of total population) between different spine categories before and after cLTP induction. (**a**) four class analysis, (**b**) three class analysis (by combining Spine-head Protrusions with Filopodia) (Color version of this figure is available at *Bioinformatics* online.)

3.3 Reproducibility analysis

In this section, we present both qualitative and quantitative analysis of multiuser reproducibility of the 2dSpAn tool to assess the reliability and robustness of the developed software. The reproducibility analysis is performed on the two image datasets from three mutually blinded independent experimental biologists. In the first image, 112 spines are segmented by each of the users in both T0 and T10 images. In the second image, 39 spines are segmented in T0 and T10 images by the independent experts using our custom designed 2D graphical interface.

Segmented images of dendritic spines from T10 by three different users are illustrated in Figure 9. Although segmentation results show significant similarity, there are some mismatches in classification results. For example, in case of segmented spine#9, results from user#1 automatically annotates it as Spine-head Protrusion, whereas the results from user#2 and user#3 annotate the same spine as Filopodia. Similarly, there are some mismatches in the classification results in spine#12, 13, 28, 41, 47, etc. The reason behind such disagreements may be illustrated from the example of spine#47, where different users segment the spine in different ways leading to varying classification results for the segmented spine. The differences in segmentation results are due to the differences in the choice of the seed pixels and other segmentation parameters like binarization thresholds, etc. Also, we have some manual segmentation and joining options in our developed 2dSpAn tool, to give more controls to the users. Uses of these advanced controls/parameters often lead to differences in segmentation and classification results.

For quantitative evaluation of the reproducibility, we have used the statistical SD of the *area* estimates of individual spines by the three independent users. In T0 and T10 images, the average SD values are observed as 0.09 and 0.07, respectively (see Supplementary Fig. S4 for detailed analysis).

3.4 Accuracy analysis and comparison with prior works

For accuracy analysis, we first generated GT spine segmentation results for all the nine neuronal images using the open source image processing software called Fiji (Schindelin *et al.*, 2012). Although, Fiji is a general purpose image analysis tool and not capable of extracting morphological attributes specific to a dendritic spine, we have considered the most generic and one of the most significant features, *area* of a spine (in micron^2), for comparative analysis. For accuracy assessment of the features, we have used *mean absolute error* (MAE) to measure the differences of the 2dSpAn estimates with respect to the GT annotations. We measure the MAE for *area* with respect to Fiji based GT annotations as, $\mathrm{MAE}_{\mathrm{area}}^{|2\mathrm{dSpAn-GT}|} = \frac{1}{n}\sum_{i=1}^{n}\left|f_i^{2\mathrm{dSpAn}} - y_i^{\mathrm{GT}}\right|$, where, n is the total number of spines, f_i and y_i are the *area* estimates of the i^{th} spine by 2dSpAn and Fiji based GT annotations, respectively. The

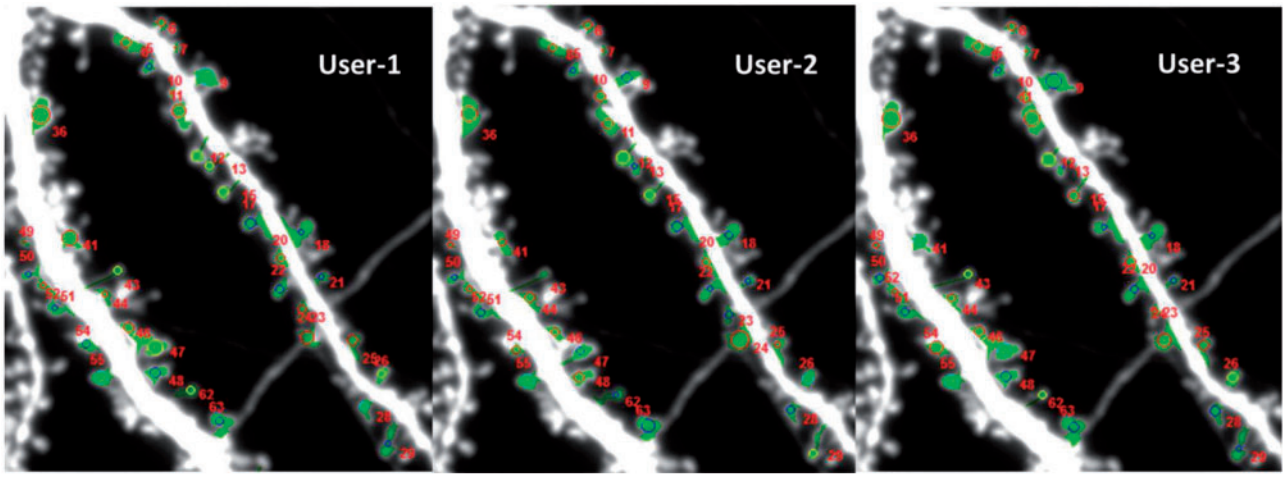

Fig. 9. Segmented images of dendritic spines from three mutually blind users (Color version of this figure is available at *Bioinformatics* online.)

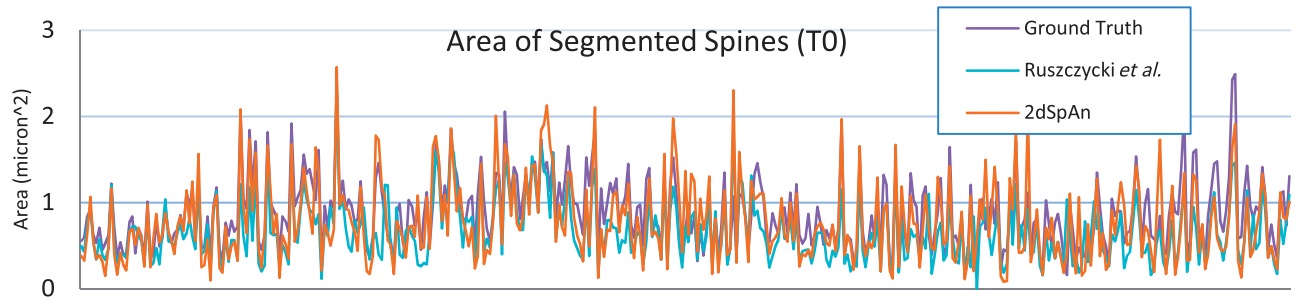

Fig. 10. Comparative accuracy analysis of the *area* feature on all the segmented spines at baseline (T0), with respect to the manually annotated GT and the results obtained by the software developed by Ruszczycki *et al.* (Color version of this figure is available at *Bioinformatics* online.)

MA $E_{area}^{|2dSpAn-GT|}$ values for 459 spines over T0 and T10 images are obtained as 0.23 and 0.21, respectively. The *SD* of errors over T0 and T10 images are observed as 0.18 and 0.19, respectively. To compare with the prior works, we have extensively evaluated the spine segmentation and annotation tool developed by Ruszczycki *et al.* (2012a,b) over all the images. Although there are significant differences in the working principal and user intervention, we found this software as the closest match with the work developed by us. Please note that, the work by Ruszczycki *et al.* use extensive manual intervention for segmentation of individual spines. The MA $E_{area}^{|Ruszczycki\ et\ al.-GT|}$ for T0 and T10 are obtained as 0.26 and 0.24, respectively. The *SD* of errors over T0 and T10 images are observed as 0.21 and 0.17, respectively. Likewise, MA $E_{area}^{|2dSpAn-Ruszczycki\ et\ al.|}$ values for T0 and T10 are estimated as 0.22 and 0.21, respectively. We also estimated and compared the *length* of the spine with respect to the work by Ruszczycki *et al.* Manual annotations in Fiji could not effectively estimate length of individual spines. $MAE_{length}^{|2dSpAn-Ruszczycki\ et\ al.|}$ values for T0 and T10 are estimated as 0.25 and 0.37, respectively. Figure 10 shows the comparative plot of the *area* feature estimated by our developed 2dSpAn tool, the Ruszczycki *et al.* software and Fiji based GT annotations over the segmented spines in the complete image set (T0). The accuracy analysis shows that the developed 2dSpAn tool is more accurate than the work by Ruszczycki *et al.* with respect to the estimated *area* of the segmented spines on both T0 and T10 images. Also, 2dSpAn requires considerably less user involvement in comparison to the work by Ruszczycki *et al.* (2012a,b)Therefore, large number of spines can be annotated quickly and effortlessly without compromising on the accuracy of the estimated spine features.

We have also assessed the accuracy of the spine classification results with respect to the manual annotations done by the one experimental neurobiologist. The spines are annotated in three classes as Mushroom, Stubby or Filopodia. 2dSpAn successfully classified 63.7% spines in T0 and 60.4% spines in T10 images. In many cases, the manual annotator was unsure about the true label of the segmented spine, thus a consensus of manual annotators would be required to improve the quality of the manual annotations. Also, automatic spine classification module itself may be improved in the future by incorporating advanced machine learning algorithms.

4 Discussion

In this work, we present a new tool for fast and accurate annotation of dendritic spines from confocal microscopy images. However, the 2dSpAn method allows determining the morphology of spines from super-resolution microscopy and is not limited only to confocal images. Please note that, the applied confocal imaging technique provides sufficient resolution to detect the changes of dendritic spines morphology (Szepesi *et al.*, 2014). We also define and extract several morphological features from the segmented spine images for quantitative assessment of spine structural plasticity. Although there are some tools that serve somewhat similar purposes, like the one developed by Ruszczycki *et al.* (2012a,b), they do not provide the

formal morphological definitions to different spine compartments. For example, there were no formal morphological characterizations to *base*, *neck* and *head* of a spine, in the prior works. There are plenty of biological discussions in contemporary literature but most of them are subjective with respect to digital image segmentation and analysis. We also provide an automatic spine classification framework based on the features extracted from the segmented spines. The proposed spine classification model works on a rule-based decision tree framework and may be improved further in future versions of the software. The performance of the classifier is assessed by comparing the manual annotations from experimental biologists. The developed spine segmentation methodology is based on a novel convolution kernel-based approach. This methodology is effective in isolating the dendritic segment in between two manually embedded seed points on the image, using the 2D graphical user interface of the developed software. The spines on either side of the dendritic segment are marked by the user by placing a single inside seed, leading to segmentation of the spine from the dendritic segment. The morphological features like *area* and *length* of the spine are computed immediately. Other features like *neck-length*, *neck-width* and *head-width* are also estimated for each segmented spine. The segmentation and classification steps in the 2dSpAn tool are extremely fast and almost instantaneous on a standard desktop computer. The segmentation task takes ~1 s and the classification of individual spines takes several milliseconds computation time on the desktop computer used in our experiment.

To assess the efficacy of the developed tool, we first analyzed dendritic spine structural changes with respect to two image datasets, before and after cLTP. We have quantitatively assessed the transitions between the spine categories Stubby, Filopodia, Mushroom and Spine-head Protrusions. The changes in spine *area* and *length* are observed over all segmented spines. For all non-Stubby spines, the changes in *neck-length* and *neck-width* values are analyzed. We have also assessed the changes in *head-width* in all Mushroom type spines. Please note that the objective of this study is to demonstrate the capabilities of the developed 2dSpAn tool and therefore we are not inferring any biological significance from the experimental observations.

For stability and robustness study, a three-user reproducibility analysis has been performed. Both qualitative and quantitative analysis show exciting results on the T0 and T10 image sets. The accuracy analysis is performed with respect to the manually annotated GT dataset and also with respect to the prior works available in this domain. There are still scopes for improvement especially with respect to the design of the user interface and also with respect to the preprocessing steps for the image sets. The complete work depends on the binarization algorithm applied on the ROI marked by the user. At this moment, we use a global binarization on the complete region. This process may sometime inflict noise in the data, leading to inappropriate segmentation of the spines. We are currently working on that issue and hope to improve the same in the upcoming version of the software. The basic software architecture, along with a representative screenshot (Supplementary Fig. S5) is discussed in supplementary and also in the user manual. Finally, on the availability of the developed software, we would like to mention that the complete open-source, platform-independent package is available at https://sites.google.com/site/2dspan/ for non-commercial use by the research community.

Funding

S.B. and S.S. were supported by Erasmus Mundus Mobility with Asia-West grant from E.U. S.B. was also supported by FASTTRACK grant [SR/FTP/ETA-04/2012] by Department of Science and Technology, Government of India. D.P. was supported by the Polish National Science Center [Grant number 2013/09/B/NZ2/00121 and 2014/15/B/ST6/05082] and COST BM1405 and BM1408 EU actions. J.W., M.R., M.M. and E.B. were supported by the National Science Center [grant number UMO-2012/06/M/NZ3/00163, UMO-2013.09/N/NZ3/03527].

Conflict of Interest: none declared.

References

Abràmoff,M.D. *et al.* (2004) Image processing with imageJ. *Biophotonics Int.*, **11**, 36–41.

Adams,R. and Bischof,L. (1994) Seeded region growing. *Pattern Anal. Mach. Intell. IEEE Trans.*, **16**, 641–647.

Alvarez,V.A. and Sabatini,B.L. (2007) Anatomical and physiological plasticity of dendritic spines. *Annu. Rev. Neurosci.*, **30**, 79–97.

Araya,R. *et al.* (2014) Activity-dependent dendritic spine neck changes are correlated with synaptic strength. *Proc. Natl. Acad. Sci.*, **111**, E2895–E2904.

Basu,S. *et al.* (2007) Text line extraction from multi-skewed handwritten documents. *Pattern Recogn.*, **40**, 1825–1839.

Bonhoeffer,T. and Yuste,R. (2002) Spine motility: phenomenology, mechanisms, and function. *Neuron*, **35**, 1019–1027.

Borgefors,G. (1986) Distance transformations in digital images. *Comput. Vision Graph. Image Process.*, **34**, 344–371.

Bourne,J.N. and Harris,K.M. (2008) Balancing structure and function at hippocampal dendritic spines. *Annu. Rev. Neurosci.*, **31**, 47.

Chang,H.T. (1952) Cortical neurons with particular reference to the apical dendrites. In: *Cold Spring Harbor Symposia on Quantitative Biology*. Cold Spring Harbor Laboratory Press, pp. 189–202.

Crick,F. (1982) Do dendritic spines twitch? *Trends Neurosci.*, **5**, 44–46.

Donohue,D.E. and Ascoli,G.A. (2011) Automated reconstruction of neuronal morphology: an overview. *Brain Res. Rev.*, **67**, 94–102.

Gray,E.G. (1959) Electron microscopy of synaptic contacts on dendrite spines of the cerebral cortex. *Nature*, **183**, 1592–1593.

Halavi,M. *et al.* (2012) Digital reconstructions of neuronal morphology: three decades of research trends. *Front. Neurosci.*, **6**, 49. doi: 10.3389/fnins.2012.00049. eCollection 2012.

Harris,K.M. (1994) Dendritic Spines. In: *eLS*. John Wiley & Sons, Ltd. doi: 10.1038/npg.els.0000093.

Heck,N. *et al.* (2015) A new automated 3D detection of synaptic contacts reveals the formation of cortico-striatal synapses upon cocaine treatment in vivo. *Brain Struct. Funct.*, **220**, 2953–2966.

Holtmaat,A. and Svoboda,K. (2009) Experience-dependent structural synaptic plasticity in the mammalian brain. *Nat. Rev. Neurosci.*, **10**, 647–658.

Lee,K.F.H. *et al.* (2012) Examining form and function of dendritic spines. *Neural Plast.*, **2012**, doi: 10.1155/2012/704103.

Matsuzaki,M. *et al.* (2001) Dendritic spine geometry is critical for AMPA receptor expression in hippocampal CA1 pyramidal neurons. *Nat. Neurosci.*, **4**, 1086–1092.

Matsuzaki,M. *et al.* (2004) Structural basis of long-term potentiation in single dendritic spines. *Nature*, **429**, 761–766.

Mishchenko,Y. *et al.* (2010) Ultrastructural analysis of hippocampal neuropil from the connectomics perspective. *Neuron*, **67**, 1009–1020.

Mukai,H. *et al.* (2011) Automated analysis of spines from confocal laser microscopy images: application to the discrimination of androgen and estrogen effects on spinogenesis. *Cereb. Cortex*, **21**, 2704–2711.

Nusser,Z. *et al.* (1998) Cell type and pathway dependence of synaptic AMPA receptor number and variability in the hippocampus. *Neuron*, **21**, 545–559.

Oh,W.C. *et al.* (2013) Synapse-specific and size-dependent mechanisms of spine structural plasticity accompanying synaptic weakening. *Proc. Natl. Acad. Sci.*, **110**, E305–E312.

Otsu,N. (1975) A threshold selection method from gray-level histograms. *Automatica*, **11**, 23–27.

Papa,M. *et al.* (1995) Morphological analysis of dendritic spine development in primary cultures of hippocampal neurons. *J. Neurosci.*, **15**, 1–11.

Ramon y Cajal,S. Textura del Sistema Nervioso del Hombre y de los Vertebrados. Vol. 2. Nicolas Moya, Madrid.

Ruszczycki,B. *et al.* (2012a) Method and a system for processing an image comprising dendritic spines. *U. S. Pat. Appl.*, **14**/237,352.

Ruszczycki,B. *et al.* (2012b) Sampling issues in quantitative analysis of dendritic spines morphology. *BMC Bioinformatics*, **13**, 213.

Saha,P. *et al.* (2015) Digital topology and geometry in medical imaging: a survey. *Med. Imaging IEEE Trans.*, **34**, 1940–1964.

Sala,C. and Segal,M. (2014) Dendritic spines: the locus of structural and functional plasticity. *Physiol. Rev.*, **94**, 141–188.

Schindelin,J. *et al.* (2012) Fiji: an open-source platform for biological-image analysis. *Nat. Methods*, **9**, 676–682.

Shepherd,G.M. (1996) The dendritic spine: a multifunctional integrative unit. *J. Neurophysiol.*, **75**, 2197–2210.

Son,J. *et al.* (2011) Morphological change tracking of dendritic spines based on structural features. *J. Microsc.*, **241**, 261–272.

Szepesi,Z. *et al.* (2014) Synaptically Released Matrix Metalloproteinase Activity in Control of Structural Plasticity and the Cell Surface Distribution of GluA1-AMPA Receptors. *PLoS One*, **9**, e98274.

Tønnesen,J. *et al.* (2014) Spine neck plasticity regulates compartmentalization of synapses. *Nat. Neurosci.*, **17**, 678–685.

Wong,S.T.C. *et al.* (2006) Methods and systems for the analysis of 3d microscopic neuron images. *U. S. Pat. Appl.*, PCT/US2006/019589.

Yuste,R. (2011) Dendritic spines and distributed circuits. *Neuron*, **71**, 772–781.

Yuste,R. *et al.* (2000) From form to function: calcium compartmentalization in dendritic spines. *Nat. Neurosci.*, **3**, 653–659.

Yuste,R. and Bonhoeffer,T. (2001) Morphological changes in dendritic spines associated with long-term synaptic plasticity. *Annu. Rev. Neurosci.*, **24**, 1071–1089.